Nanotechnology **19** (2008) 225305 (9pp) doi:10.1088/0957-4484/19/22/225305

Growth behavior near the ultimate resolution of nanometer-scale focused electron beam-induced deposition

W F van Dorp[1,3], C W Hagen[1], P A Crozier[2] and P Kruit[1]

[1] Delft University of Technology, Faculty of Applied Sciences, Lorentzweg 1, 2628 CJ Delft, The Netherlands
[2] Center for Solid State Science, Arizona State University, Tempe, AZ 85287, USA

E-mail: w.f.vandorp@tudelft.nl

Received 10 December 2007
Published 25 April 2008
Online at stacks.iop.org/Nano/19/225305

Abstract

An attempt has been made to reach the ultimate spatial resolution for electron beam-induced deposition (EBID) using $W(CO)_6$ as a precursor. The smallest dots that have been written have an average diameter of 0.72 nm at full width at half maximum (FWHM). A study of the nucleation stage revealed that the growth is different for each dot, despite identical growth conditions. The center of mass of each dot is not exactly on the position irradiated by the e-beam but on a random spot close to the irradiated spot. Also, the growth rate is not constant during deposition and the final deposited volume varies from dot to dot. The annular dark field signal was recorded during growth in the hope to find discrete steps in the signal which would be evidence of the one-by-one deposition of single molecules. Discrete steps were not observed, but by combining atomic force microscope measurements and a statistical analysis of the deposited volumes, it was possible to estimate the average volume of the units of which the deposits consist. It is concluded that the volume per unit is as small as 0.4 nm^3, less than twice the volume of a single $W(CO)_6$ molecule in the solid phase.

(Some figures in this article are in colour only in the electronic version)

1. Introduction

Developing techniques for the controlled fabrication of nanostructures is a topic of intense research and is critical to exploit the full potential of nanotechnology. Focused electron beam-induced processing (FEBIP) can be used to define and precisely position arbitrary shaped patterns onto substrates. Precursor molecules, introduced into a vacuum chamber, adsorb on the substrate and are irradiated by a focused electron beam (e-beam). Under the influence of the e-beam, the adsorbed molecules are dissociated into fragments. If these fragments react with the substrate and form volatile species, the substrate is etched (in the case of electron beam-induced etching, EBIE). If the fragments stick to the surface and form a deposit, one speaks of electron beam-induced deposition (EBID). Since the fragmentation only occurs in or very close to the irradiated area and electron beams can be made as small as 0.1 nm, EBID is very well suited for sub-10 nm patterning. This has been demonstrated with deposits having widths of 8 nm [1, 2], 5 nm [3], 4 nm [4], 3.5 nm [5], 1.5 nm [6] and even 1.0 nm [7]. The patterning capabilities are demonstrated with a world map that includes topographical information (see figure 1). The color indicates that the Himalayas, the Rocky Mountains and the Andes are higher than the rest of the world. Honduras is 7.5 nm wide.

It has already been shown that for sub-5 nm deposits, the amount of deposited material is not constant, but fluctuates (even for identical fabrication conditions) [7]. It was estimated that a deposit with a diameter of about 2 nm contains a number of molecules in the order of 80 [8]. This indicates that the number of molecules dominates the statistics, rather than the number of electrons required for the dissociation. It has also been shown earlier that *in situ* measurements of the annular dark field (ADF) signal give valuable insight into the growth process and can even allow control over the deposition of lines [9]. Measuring the ADF signal *in situ* is in

[3] Author to whom any correspondence should be addressed.

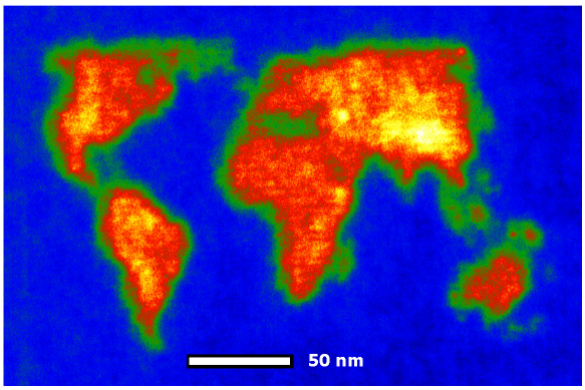

Figure 1. World map created with EBID. The false colors indicate that the Himalayas, the Rocky Mountains and the Andes are higher than the rest of the world.

principle similar to recording the sample current during deposit growth as performed by Bret *et al* [10], although the ADF signal can be measured for electron transparent (i.e. very thin) samples only. The advantage, however, is that the sensitivity of the ADF signal to the amount of deposited material is greater. It is possible to image single W atoms with the ADF signal [11]. In [9], $W(CO)_6$ was used as a precursor and it was estimated that the ADF signal sensitivity during the deposition experiments was a single $W(CO)_x$ molecule. In the present article, the nucleation stage of sub-10 nm EBID growth from $W(CO)_6$ is explored. To perform this study, measurements of the ADF signal during the growth and post-deposition ADF image processing were combined with atomic force microscope (AFM) measurements.

2. Experimental details

EBID was performed in an environmental Tecnai F20 scanning transmission electron microscope (STEM), allowing the entire growth process to be observed and controlled *in situ* and in real time. The microscope is equipped with a field-emission electron source and was operated at 200 keV with a nominal beam spot size of 0.3–0.4 nm. Details of the microscope and the precursor supply system are given elsewhere [12]. The precursor used for deposition was $W(CO)_6$, and typical pressures were in the region of 1×10^{-3} Torr. Substrates were 10 nm thick amorphous carbon and 50 nm thick Si_3N_4 membranes. During experiments, the substrate was kept at a temperature of 150 °C to reduce the effect of contamination.

Imaging was performed with the annular dark field (ADF) signal. For thin films, the ADF image intensity is linear with mass or thickness and is given in counts (arbitrary units). All depositions were done on an area that was not previously exposed to electrons.

Arrays of dots were deposited with two different scan routines. Suppose for instance that EBID was performed on three positions on the substrate, positions I, II and III (marked with + in figures 2(a) and 3(a)). In scan routine A (figure 2(a)), the positions were irradiated sequentially with the beam in a stationary position for a specific dwell time (for instance 1000 ms).

In scan routine B, the beam was scanned over position I (see figure 3(a)). The scan area was 2×2 nm in size, divided into 5×5 pixels, and the dwell time $t_{\mathrm{dwell,scanning}}$ was 10 μs per pixel. The time required for one frame, t_{frame}, was therefore 0.25 ms. During the scan, the ADF signal was collected and the intensity I_{scan} (integrated over the 5×5 pixels) was saved

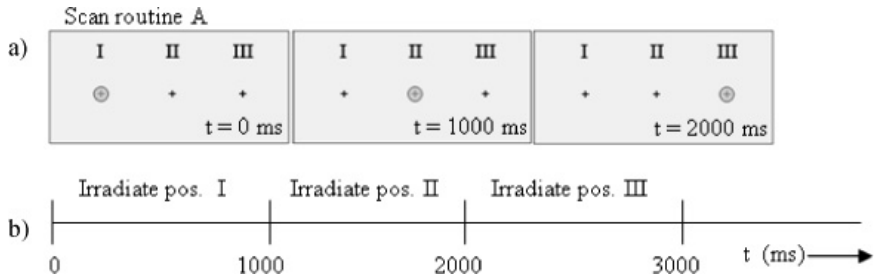

Figure 2. (a) Schematic drawing of scan routine A. The e-beam is focused onto position I and kept stationary during the dwell time (1000 ms). Sequentially, position II and position III are irradiated. (b) Corresponding time line.

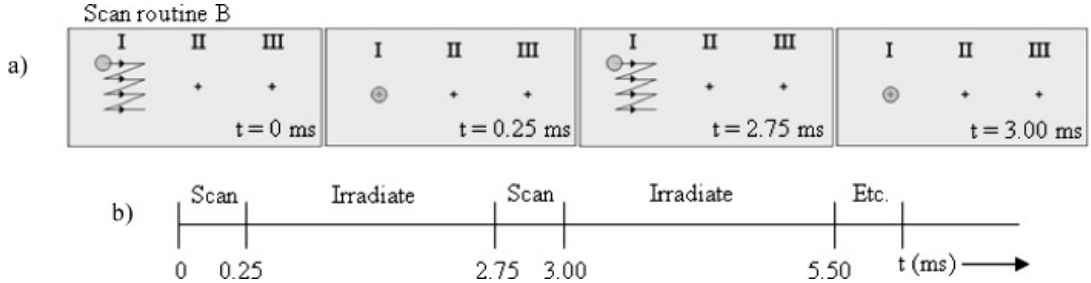

Figure 3. (a) Schematic drawing of scan routine B. First, the beam is scanned over position I, during which the ADF signal is collected. Next, the beam is kept stationary on position I for a given dwell time. This scan sequence of scanning (and collecting the ADF signal) and irradiating is repeated on position I for a number of iterations, after which the entire procedure is repeated for positions II and III.
(b) Corresponding time line (not to scale).

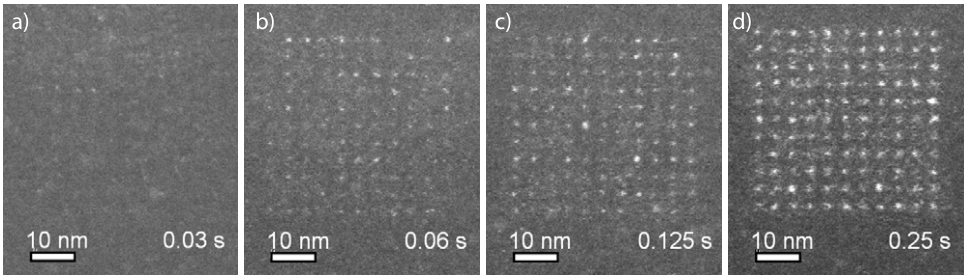

Figure 4. Four 11 × 11 arrays deposited with scan routine A, using different dwell times. As the dwell time increases, the amount of deposited material also increases (visible as an increase in dot intensity).

to file. Next, position I was irradiated by keeping the beam stationary in the center of the 2×2 nm^2 square. The irradiation time $t_{\text{irradiate}}$ was chosen such that $t_{\text{irradiate}} = 10 \times t_{\text{frame}}$, so $t_{\text{irradiate}}$ was 2.5 ms. This scan sequence (scanning, saving and irradiating) was repeated for a number of iterations (100, 200 or 400), after which the procedure was repeated for positions II and III.

Both scan routines were performed with a constant dwell time (routine A) or a constant number of iterations (routine B) per array. At the end of the routines, the beam was blanked. During the writing of the arrays, the environmental cell was flooded with precursor gas. ADF images of the completed arrays were not taken until the precursor gas was pumped out (unless mentioned otherwise).

Dedicated hardware and software were developed to use scan routine B on the environmental STEM. Scan signals were generated with a National Instruments (NI) card and added with an adding amplifier to the scan signals of the standard microscope control. The maximum scan rate that could be achieved was limited by the hardware of the microscope. It was found that for dwell times per pixel <10 μs the pattern was no longer defined correctly.

The ADF signal was recorded using the same NI card. The minimum sampling time for the NI card was 1 μs. This means that for a $t_{\text{dwell,scanning}}$ of 10 μs per pixel, the ADF signal was integrated over 10 samples.

3. Image analysis

In order to collect data from the EBID experiments, a technique to analyze the ADF images of the deposited arrays was developed. This technique is used to determine the diameter of the deposits and to determine the integrated intensity of each deposit, I_{dot}. In each array (11 × 11 or 7 × 7), the dots were intended to be deposited on a square grid. However, the arrays are distorted because of drift of the specimen during deposition. To correct for this, a trapezium-shaped grid is overlaid on the ADF image, such that the points of the grid coincide as best as possible with the dot positions in the array.

For measurements of the deposit diameters, a box is overlaid on each point of the trapezium-shaped grid, centered around the grid point. Each box is $n \times n$ pixels and is now a sub-image, containing the ADF image of a single dot. All boxes (i.e. all sub-images of the single dots) are added linearly, which yields an average ADF image (of $n \times n$ pixels) of the dots in the array. In this averaged sub-image, the center of gravity of the dot is determined, which is used to measure the average diameter.

For the measurement of I_{dot}, two boxes are overlaid on each point of the trapezium-shaped grid, centered around the grid point. Box 1 contains N_1 pixels and is large enough to overlap the area covered by the dot including its tails. Box 2 contains N_2 pixels and is slightly larger than box 1. Then, the sums ΣI_1 and ΣI_2 of all intensity values of respectively box 1 and box 2 are calculated. The average background intensity value per pixel I_{BG} is calculated by

$$I_{\text{BG}} = (\Sigma I_2 - \Sigma I_1)/(N_2 - N_1). \quad (1)$$

The integrated intensity arising from the deposited material I_{dot} on a particular grid point is calculated by

$$I_{\text{dot}} = \Sigma I_1 - (I_{\text{BG}} * N_1). \quad (2)$$

The procedure of overlaying the boxes and calculating I_{dot} is performed for all dots in the array. Since the pixel intensity in ADF images is proportional to the thickness of the probed area, I_{dot} (in arbitrary units) is proportional to the volume of the deposit.

4. Results and discussion

Arrays with dwell times of 0.25, 0.125, 0.06 and 0.03 s have been deposited on a 10 nm thick amorphous carbon substrate with scan routine A. ADF images were recorded with the precursor gas present. The results are shown in fig 4. There are a number of observations to make on arrays obtained with scan routine A concerning (1) the average amount of deposited material, (2) the diameter of the dots, (3) the shape of the dots, and (4) the positions of the dots with respect to the intended grid position. Starting with the amount of deposited material, it is observed that the amount of deposited material increases with increasing dwell time. This is visible in the ADF images as an increase in dot intensity. I_{dot} was determined for the arrays in figure 4 and is found to increase linearly with dwell time (see figure 5(a)).

Of the arrays shown in figure 4, the averaged sub-images have been taken and are shown in figures 5(b)–(e).

From these averaged sub-images, the dot diameter d_{dot} is determined. Figure 5(a) shows the full width at half maximum (FWHM) and the FW50% (the diameter in which 50% of the

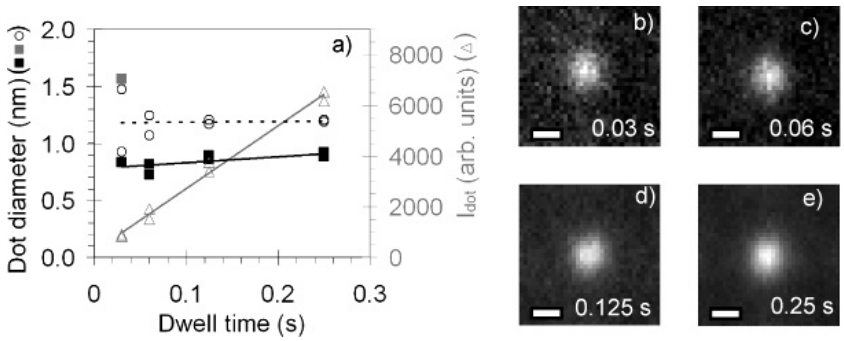

Figure 5. (a) A plot of I_{dot} (△), the FWHM (■) and FW50% (○) as a function of the dwell time. The gray point is considered an outlier and is not used to fit the trendline for the FWHM. (b)–(e) The average sub-images of the dots. The scale bars indicate 1 nm.

dot volume is contained). It is observed that d_{dot} (FWHM) decreases from 0.90 nm to 0.83 nm for dwell times of 0.25 and 0.03 s, respectively. The smallest diameter measured is 0.72 nm for the FWHM and 1.0 nm for the FW50%. The outlier for the smallest dwell time (shown in gray) is the result of the difficulty in determining the center of gravity in the averaged sub-images. The noise level in the sub-images becomes significant because so little material was deposited (see figure 5(a)).

An average diameter of 1.0 nm for the smallest FW50% is the smallest that has been achieved until now. It is also close to the value that was predicted by a Monte Carlo simulation. In [13], results are described from a simulation of the scattering of 200 keV primary electrons in a flat, 10 nm thick Cu sample. It turns out that, for a 0.2 nm diameter electron beam, 50% of the secondary electrons are emitted from an area 0.86 nm in diameter. Although a different substrate was used in the experiment, it shows that the smallest average diameter in the experiment is very close to the ultimate EBID resolution.

The limit in spatial resolution for the average deposit may have been nearly reached; individual deposits can still be smaller than 0.86 nm. The smallest conceivable individual deposit is a single molecule. The factor currently limiting the average deposit diameter is the positioning precision, because the center of mass of each dot is not exactly on the intended position in the array. This can be due to several effects. First of all, the area from which secondary electrons are emitted from the substrate is larger than the diameter of a single molecule. Secondly, it is possible that molecules diffuse between the moment that they are dissociated and the moment that they are actually pinned down. The result of these two effects is that the deposit nucleates on a random spot close to the irradiated spot. Figure 6 shows a schematic drawing of three irradiated positions on the substrate (I, II and III). Supposing that the electron beam irradiates the substrate at +, secondary electrons are emitted from the area around it (shown in gray). The deposit does not necessarily nucleate on +, but can for instance nucleate on position 1, 2 and 3. Although the individual deposits may be single molecules in each case, the average diameter will be larger. Finally, other factors contributing to the average diameter are specimen drift and (possibly) small vibrations in the electron beam during writing and imaging of the deposit. The average distance between the intended

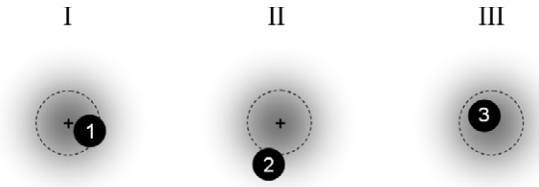

Figure 6. Schematic drawing of three irradiated positions on the substrate (I, II and III). The electron beam irradiates the substrate at +, around which secondary electrons are emitted (shown in gray). The deposit nucleates on a random position in an area around '+'. The average distance between the intended position in the array and the center of mass of the dot is indicated with the dashed circle in figure 6, and is 0.23 nm for the dots in figure 4.

position in the array and the center of mass of the dot is indicated with the dashed circle in figure 6, and is 0.23 nm for the dots in figure 4. From the fact that this distance is smaller than the FW50% of the secondary electron (SE) emission area, it is concluded that under these conditions diffusion does not play a significant role in determining the limit of the spatial resolution.

It appears that not only the first nucleus is deposited on a random position. Later on in the process, material can still be deposited on random positions around the irradiated spot. This becomes evident from the ADF images in figure 7. Dots are shown for three different dwell times. The deposition conditions were similar (though not identical) to the conditions used to create the arrays in figure 4. Per dwell time, the dots were taken from the same array, so the deposition conditions were identical. The white squares indicate 5 nm × 5 nm. It is clearly observed that the dots are nonsymmetric and all different from each other. The nonsymmetry of the dots implies that the definition of the size of an individual deposit becomes difficult.

The results discussed until now are based solely on arrays deposited with scan routine A. An attempt to use this scan routine A to control variations in the mass of dots was not successful [9]. The explanation given was that 'a significant part of the dot grows nonsymmetrically outside the area exposed by the electron beam'.

To be able to probe the entire dot and detect the deposition of single molecules, scan routine B was developed. Typical

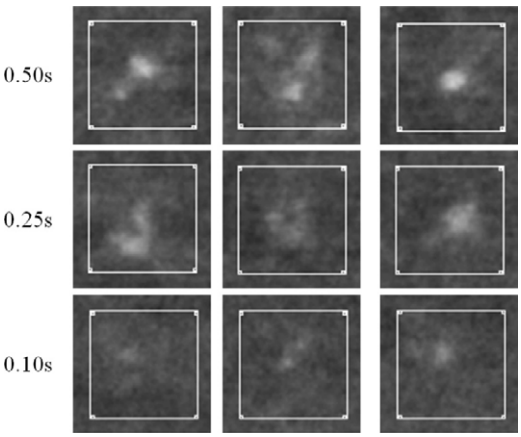

Figure 7. Close-up of some of the dots. The white squares indicate 5 nm × 5 nm. Many of the dots are nonsymmetric. The time on the left is the dwell time.

developments of I_{scan} as a function of time are shown in figures 8(a)–(e). The raw data are presented in gray, and the averaged data (moving average over 35 data points) are presented in black. Figure 8(a) shows a measurement of the noise, recorded by executing scan routine B in the absence of precursor gas. The standard deviation of I_{scan} for this measurement is 4.1 mV. Figures 8(b)–(e) are measurements with precursor gas. Figure 8(f) is the average curve for 147 deposits, which shows that the average increase in I_{scan} is about 17 mV. This means that the strong increases observed in figures 8(c) and (e) are outliers and not typical of the deposition process. It is observed that the growth rate is not constant during the deposition. During the periods indicated with A, C and E the ADF signal stays roughly constant for as much as tenths of seconds. There are gentle (C and F) and stronger (D) increases, and even decreases (G) of the ADF signal. Occasionally, sharp changes in the signal are observed. Examples of these sharp changes are indicated with black lines in figures 8(d) and (e). The values are averages over the width of the lines.

The average growth curve in figure 8(f) makes clear that the growth in the very early stage is not linear (assuming that the composition remains constant). A similar nonlinearity was observed by Guise *et al* [14]. It is tentatively suggested that this is due to the change in target surface during the first stages of growth. As the deposit grows, the surface onto which precursor molecules adsorb changes from substrate to deposit. The resulting change in residence time of precursor molecules and/or SE yield can lead to lower growth rates later on.

What are the sharp changes observed in figures 8(d) and (e)? Are they deposition of single molecules? If so, what do the more gentle changes in figure 8(b) and (c) mean? To answer these questions, it is important to characterize the deposits in more detail. In the first place, this is done by determining the height of the deposits with an AFM. Secondly, the variations in deposit mass are analyzed. In figure 4, it is observed that the dot intensity (i.e. the deposited mass) is not constant over the array. There is a variation in intensity, even though the deposition conditions were identical for each dot in the array. A better understanding of these variations may be helpful for interpreting the growth curves in figure 8.

To be able to probe the dots with an AFM, dots were deposited on a 50 nm thick Si_3N_4 membrane with a beam current of 36 pA. The results are shown in figure 9. The insets in (a), (b) and (c) show a schematic representation of the orientation of the sample with respect to the electron beam or the AFM tip. In the transmission microscope, the recorded images give a projection of the sample. Assuming that the composition of the deposit is constant, the highest point of the

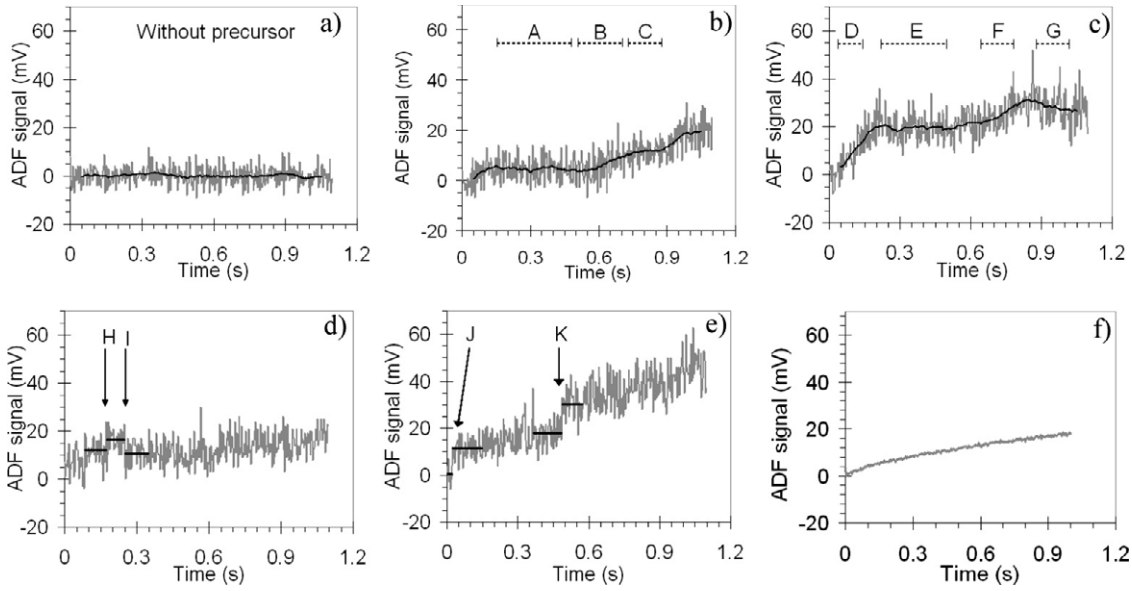

Figure 8. (a) Scan routine B executed without precursor gas present. No deposition is observed, which allows the determination of the noise level. ((b), (c), (d), (e)) Scan routine B executed with precursor gas present. Curves shown in gray are raw data; curves shown in black are averaged data. Averaging for ((b), (c)) was over 35 data points; averaging for ((d), (e)) was over the width of the indicated lines. Indicated are periods of no significant growth (A, C, E), increases (C, D, F), a decrease (I) and sudden jumps (H, J, K).(f) Data averaged over 147 growth curves.

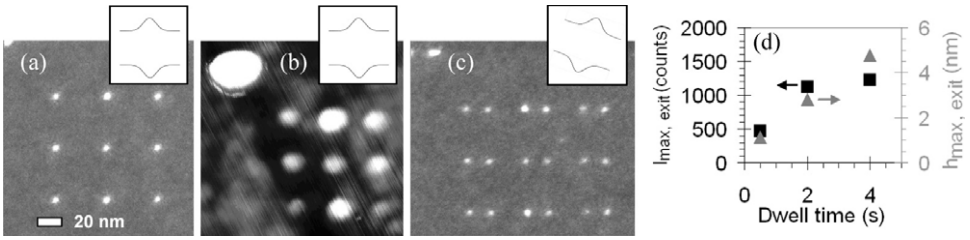

Figure 9. (a) ADF image of dots written with a beam current of 36 pA and a dwell time of 2 s per dot (perpendicular). (b) AFM image of the exit side of the array in (a). (c) ADF image of the array in (a), but now tilted to 15°. (d) $I_{max,exit}$ and $h_{max,exit}$ plotted as function of the dwell time. The insets in ((a), (b), (c)) show a schematic representation of the orientation of the sample with respect to the electron beam or the AFM tip.

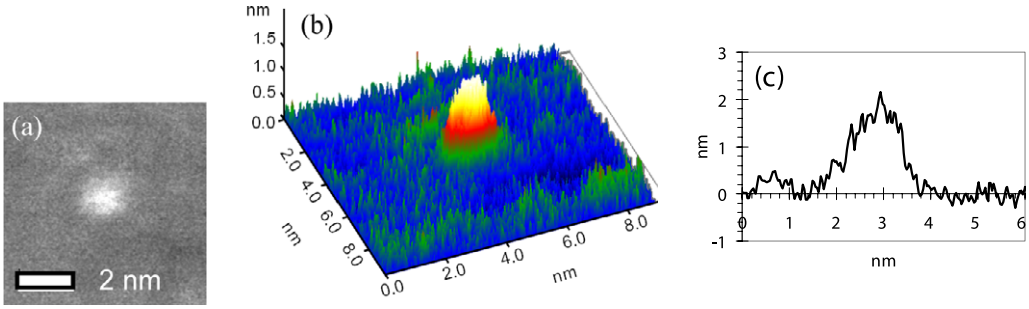

Figure 10. (a) ADF image. (b) The same ADF image, but now in 3D representation with scaling of the z-axis in nm. (c) Height profile of the dot in (a). The horizontal and vertical axes are shown with identical scaling to demonstrate the relative dimensions.

deposit is represented by the highest intensity of the deposit, I_{max}. Since EBID is performed on an electron transparent membrane, a deposit grows on the entrance as well as on the exit side, so I_{max} is the sum of the intensity of the deposit on the entrance and exit sides:

$$I_{max} = I_{max,entrance} + I_{max,exit}. \quad (3)$$

A dot array was deposited (figure 9(a)). With the AFM, only the part of the dot on the exit side of the membrane was probed (see figure 9(b)). This gives the height of the highest part of the deposit, $h_{max,exit}$. To have a measure for $I_{max,exit}$, the membrane was tilted to 15° (see figure 9(c)). From these tilted ADF images, the integrated intensities $\Sigma I_{dot,entrance}$ and $\Sigma I_{dot,exit}$ are determined. It is assumed that the growth rates at the entrance and exit sides are identical for these small deposits. In other words, it is assumed that

$$I_{max,exit} = I_{max} * [\Sigma I_{dot,exit}/(\Sigma I_{dot,entrance} + \Sigma I_{dot,exit})]. \quad (4)$$

Both $I_{max,exit}$ and $h_{max,exit}$ are averaged per array. Figure 9(d) shows these average values for three different dwell times. It is observed that $h_{max,exit}$ is linearly proportional to $I_{max,exit}$ for dwell times of 0.5 and 2.0 s. For the array deposited with 4.0 s, this is no longer the case. We suspect that at a dwell time of 4.0 s, the growth rates at the entrance and exit sides are no longer identical, because the deposit at the entrance side has become too thick. This means that relationship (4) is not valid for this array.

Assuming a constant composition, the ADF intensity is proportional to the deposit height, so the AFM measurements can be used to scale the ADF intensities (in arbitrary units) to height (in nm). Based on the values of $h_{max,exit}$ and $I_{max,exit}$ for the 0.5 and 2.0 s arrays, the scaling factor $C_{36\ pA}$ is 2.5×10^{-3} nm/count.

Figure 10(a) shows an ADF image of a deposit written on a 10 nm thick amorphous carbon substrate with a beam current of 3.2 pA. It is assumed that the ADF current decreases proportionally to the beam current. Taking into account a difference in magnification, the intensity conversion factor $C_{3.2\ pA}$ is 1.4×10^{-2} nm/count. In figure 10(b), the same ADF image is shown, but now in 3D representation with the z-axis in nm. The line profile of the dot in figure 10(a) is shown in figure 10(c). The horizontal and vertical axis are shown with identical scaling to demonstrate the relative dimensions.

With the AFM measurements, the intensity variations such as observed in figure 4 can be expressed in terms of variations in deposited volume. This has been done for arrays of dots deposited on a 10 nm thick amorphous carbon substrate, with dwell times of 1.00, 0.50, 0.25 and 0.10 s and a beam current of 3.2 pA. For each position in the array I_{dot} has been determined. For each dwell time, three 7×7 arrays have been deposited, which gives 147 measurements of I_{dot} per dwell time. I_{dot} is proportional to the volume of the deposit (in arbitrary units) and can be scaled to V_{dot} (in nm^3) using $C_{3.2\ pA}$ (in nm) and the area per pixel in the ADF images (in nm^2). Please note that V_{dot} is the sum of the volume of the deposits on the entrance and the exit sides of the membrane.

The values for V_{dot} were binned and are shown in the histogram in figure 11(a). The number of occurrences N_V has been normalized to the total number of measurements per dwell time (147). So for instance, if a V_{dot} of 1.4 nm^3 occurred 28 times in the 0.25 s arrays, this gives an N_V of $28/147 = 0.2$

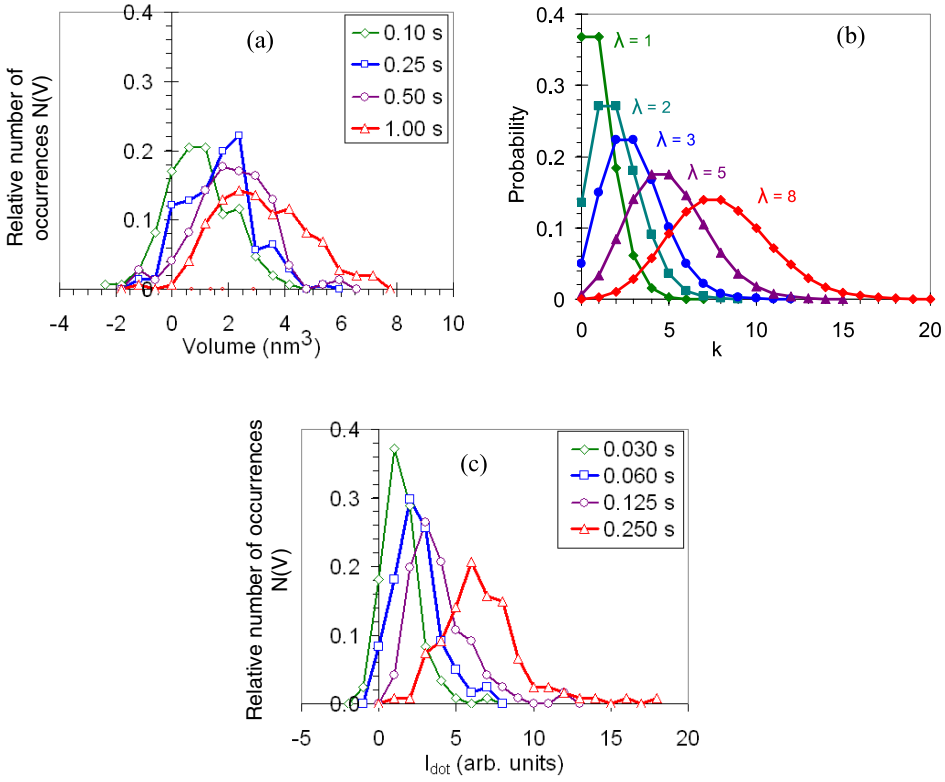

Figure 11. (a) The relative frequency with which dot volumes occur in arrays deposited with dwell times of 0.10, 0.25, 0.50 and 1.00 s. (b) Poisson statistics for expectation values λ of 1, 2, 3, 5 and 8 (lines are drawn to guide the eye and do not indicate continuity). (c) The relative frequency with which I_{dot} occurs in the arrays in figure 4.

in figure 11(a). It is observed that, as the dwell time increases, the average amount of deposited material also increases. The negative values are the result of noise in the ADF images. At the smallest dwell times, there are many positions in the array where there is very little or even no deposit and the background correction applied in equation (2) can give rise to negative values for I_{dot} (and hence negative values for V_{dot}).

The growth of a deposit consists of a series of dissociation events. If these dissociation events do not influence each other and occur at a known average rate, the volume distributions can be modeled with Poisson distributions. A Poisson distribution expresses the probability $P_{(k)}$ that a particular event occurs k times for a given expected number of discrete events (λ) during an interval of known length. Poisson distributions are calculated with

$$P_{(k)} = (\lambda^k \mathrm{e}^{-\lambda})/k!. \tag{5}$$

In the experiments described here, k represents the number of discrete units that have been deposited, or the amount of material that was deposited (V_{dot} in figure 11(a)). The probability $P_{(k)}$ corresponds to the relative number of times N_V that a particular number of units or a particular volume is found. Parameter λ then represents the average number of dissociation events for a given dwell time. The values of $P_{(k)}$ have been calculated for $\lambda = 1$, 2, 3, 5 and 8, and are shown in figure 11(b). It is observed that the shapes of the distributions in figures 11(a) and (b) are similar, with the exception of the values for 0.10 s dwell time in figure 11(a). This is probably due to the noise in the ADF images and in the image processing. The shape of these distributions is reproducible, as becomes clear from the histogram of values for I_{dot} in figure 11(c). These values were calculated from the arrays in figure 4 and, although I_{dot} was not calibrated with the AFM measurement, the trend is clearly similar to that in figure 11(b).

By fitting the Poisson distributions to the volume distributions, an estimate can be made of λ for each dwell time used in the experiments. This estimate is based on the assumption that every deposited molecule is visible in the ADF image. In figure 12(a), an example of a fit is shown. Two fit parameters were used: λ and the linear scaling factor f. The factor f merely served to scale values of k to the volumes found in the experiment. Values for $P_{(k)}$ were not scaled.

In figure 12(b) the data from the different sources are shown as function of time. The averages for V_{dot} (▲) are calculated from the distributions in figure 11(a). The fitted λ (■) and the average values for I_{scan} (same data as in figure 8(f)) are shown in gray. From figure 12(b), it is calculated that after 1.0 s deposition time the average V_{dot} is 2.9 nm^3, the scaling factor for I_{scan} is 6.1 mV nm^{-3}, the average dissociation rate R_{diss} is 5.5 λ s^{-1}, and the average volume per λ (V_λ) is 0.4 nm^3. From the beam current of 3.2 pA it is calculated that the dissociation efficiency is 3.7×10^6 electrons/λ. This value is relatively high if compared to the number of electrons needed to deposit a single $Pt(PF_3)_4$ molecule (1.8×10^3) [15] or a single $Ru_3(CO)_{12}$ molecule (280) [16]. However, it needs to be emphasized that the primary electron energy was much higher

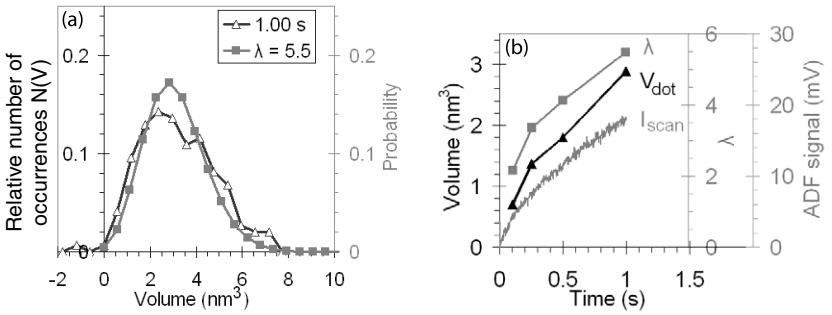

Figure 12. (a) A fit of a Poisson distribution to the volume distribution of arrays with 1.00 s dwell time. (b) The average values for V_{dot} and the fitted values for λ as function of the dwell time. The average dissociation rate after 1 s was 5.5 λ s^{-1}, and the average volume of material that is deposited per λ is 0.4 nm^3.

in our case (200 kV versus 3 or 40 kV, respectively). At 200 kV, the cross sections for dissociation (directly by the primary electrons) or for secondary electron generation are relatively small. Furthermore, it needs to be emphasized that no attempt was made for optimization of the dissociation efficiency. We tried to minimize the growth rate as far as possible to allow for sufficient time to reduce the noise on the ADF signal.

The question remains what λ is. V_λ is within a factor of 2 of the volume of a $W(CO)_6$ molecule, which is 0.22 nm^3 (calculated from the density in the solid phase, 2.65 g cm^{-3}). If λ represents one $W(CO)_x$ molecule, the fact that V_λ is so large could indicate that the fragmentation of the precursor molecules is far from complete and that most of the CO groups are still in the deposit. It can also mean that V_λ is overestimated. If the ADF signal is not sensitive enough to detect single $W(CO)_x$ molecules, the fit procedure for λ (as shown in figure 12(b)) underestimates the number of molecules per dwell time, leading to an overestimation of V_λ. It is also possible that the dissociation process does not go molecule by molecule, but that λ represents a cluster of several molecules. It is not straightforward to suggest a measurement that allows a discrimination between the two options.

In figure 13, the information from the different analysis methods is put together. Figure 13(a) shows three growth curves (on the left vertical axis nm^3, on the right vertical axis λ). In figure 13(b), the ADF images of the corresponding dots are shown. The size of the area that was scanned during scan routine B (2 × 2 nm) is indicated with the white squares overlayed on the ADF images. As a comparison to scan routine B, figure 13(c) shows an ADF image acquired after scan routine A for dots written with comparable dwell times under identical conditions. It is observed that there was some parasitic deposition during t_{frame}; the intensity in the background is clearly higher in figure 13(b) than in figure 13(c). This indicates that there was some extra (and unintended) deposition during t_{frame} in scan routine B.

Similar to the growth curves in figure 8, levels are observed in figure 13(a) where the ADF signal is (roughly) constant. If these levels were separated by a constant step size, it would suggest that the deposition of a constant volume (either single molecules or clusters of molecules) is detected. However, a detailed analysis of the data shows that the step

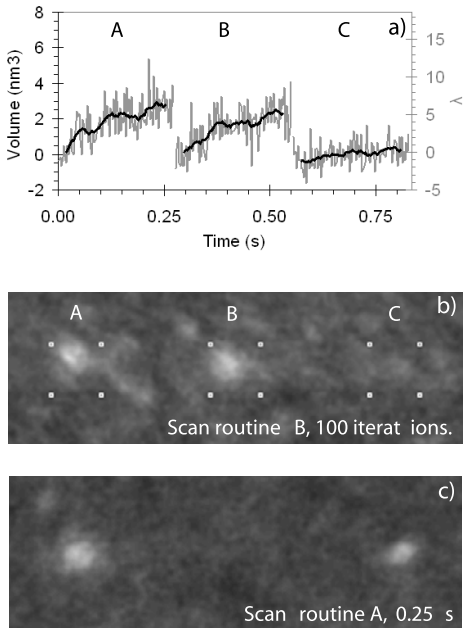

Figure 13. (a) I_{scan} as a function of time for three positions. (b) An ADF image of the dots corresponding to the growth curves in (a). The white squares indicate the size of the area scanned during scan routine B (2 × 2 nm). (c) An ADF image of dots written with scan routine A, deposited with a comparable dwell time and under identical conditions as the dots in (b).

sizes between the levels are randomly distributed. A constant step size is not detected.

The fact that steps of a constant size were not detected in the development of I_{scan} as a function of time can be due to several (parallel) effects. One possibility is that the dissociation process is not discrete. The similarity between the experimentally obtained deposit volume distributions (figures 11(a) and (c)) and the theoretical Poisson distributions (figure 11(b)) seems to indicate that the dissociation events are uncorrelated in time, but the precursor chemistry may be more complex. Another possibility is that the precursor molecule does not dissociate into fragments of a constant composition. Measurements of the composition with electron energy loss spectrometry have shown that the deposited material is not pure W. Rather, the deposits consist of fragmented $W(CO)_x$

molecules, where x can vary (theoretically speaking) from 5 to 0. The composition is important for the ADF intensity, because it scales with approximately $Z^{1.6}$ to $Z^{1.9}$ [17]. For $x = 5$, $Z_{CO5} = (6 + 8) \times 5 = 70$, which is of the same order of magnitude as Z_W (74). This means that the Z of a dissociated molecule can vary nearly continuously from 74 (Z_W) to 144 ($Z_{W(CO)5}$), smearing out (possible) steps in the ADF signal. Another possibility is that the contamination level was too high during the experiment. If the environmental cell in the microscope or the gas pipes leading to the cell were not clean enough, the co-deposition of contamination may have obscured any steps in the ADF signal. Finally, the parasitic deposition during the scanning in scan routine B may have disturbed the measurements.

Getting back to the data in figure 8, we have been able to determine the volumes of the material that was deposited during the recording of the growth curves. The growth rate varies between -3.3 and 15 nm^3 s^{-1} and the magnitude of the changes is 0.9 nm^3 (H), -1.0 nm^3 (I), 2.0 nm^3 (J) and 2.0 nm^3 (K). These values are significantly larger than V_λ (0.4 nm^3) and it is tentatively suggested that these sharp changes are clusters of molecules that move into or out of the scanned area by adsorption, desorption or diffusion during the deposition process. Although more experiments are required to determine how the ADF signal should be interpreted precisely and how it depends on precursor chemistry, it is shown that valuable insight into the deposition process can be obtained by combining measurements of the ADF signal (*in situ* and post-deposition) with AFM measurements.

5. Conclusions

The nucleation stage of EBID has been studied for deposits from $W(CO)_6$. Measurements of the ADF signal during the growth and post-deposition ADF image processing were combined with atomic force microscope measurements. The smallest average diameter measured is 0.72 nm for the FWHM and 1.0 nm for the FW50%. The average growth rate after 0.1 s of deposition time was 2.9 nm^3 s^{-1}. The development of a deposit as function of time is found to be different for each dot, despite identical growth conditions. The center of mass of each dot is not exactly on the position irradiated by the e-beam; instead, the deposit nucleates on a random spot close to the irradiated spot. Not only the first nucleus is deposited on a random position. Later on in the process, material can still be deposited on random positions around the irradiated spot. As a result of this, the shape of the dots is nonsymmetric. The growth rate is not constant during deposition (varying between -3.3 and 15 nm^3 s^{-1}) and the final deposited volume varies from dot to dot. The volume distributions found in the experiments were compared to Poisson distributions. This comparison allowed an estimation of λ, the expected number of discrete events during a specific interval. It was estimated that after 1.0 s of deposition time, the average deposition rate was 5.5 λ s^{-1}, with a volume of 0.4 nm$^3/\lambda$ and a deposition efficiency of 3.7×10^6 electrons/λ. The volume of 0.4 nm^3 is within a factor of 2 of the volume of a $W(CO)_6$ molecule in the solid phase. Despite the low growth rate, it was not possible to detect the deposition of single molecules or clusters as discrete steps in the recorded ADF signal.

Acknowledgments

We would like to thank Jacques Nonhebel and Frans Berwald for developing the hardware and software for scan routine B, and gratefully acknowledge the use of the facilities in the Center for Solid State Science at Arizona State University.

References

[1] Broers A N, Molzen W W, Cuomo J J and Wittels N D 1976 *Appl. Phys. Lett.* **29** 596
[2] Jiang H, Borca C N, Xu B and Robertson B W 2001 *Int. J. Mod. Phys.* B **15** 3207
[3] Fujita J, Ishida M, Ichihashi T, Ochiai Y, Kaito T and Matsui S 2003 *J. Vac. Sci. Technol.* B **21** 2990
[4] Crozier P A, Tolle J, Kouvetakis J and Ritter C 2004 *Appl. Phys. Lett.* **84** 3441
[5] Guise O, Ahner J, Yates J and Levy J 2004 *Appl. Phys. Lett.* **85** 2352
[6] Tanaka M, Shimojo M, Han M, Mistuishi K and Furuya K 2005 *Surf. Interface Anal.* **37** 261
[7] van Dorp W F, van Someren B, Hagen C W, Kruit P and Crozier P A 2005 *Nano Lett.* **5** 1303
[8] van Dorp W F, van Someren B, Hagen C W, Kruit P and Crozier P A 2006 *J. Vac. Sci. Technol.* B **24** 618
[9] van Dorp W F, Hagen C W, Crozier P A and Kruit P 2007 *J. Vac. Sci. Technol.* B **25** 2210
[10] Bret T, Utke I, Bachmann A and Hoffmann P 2003 *Appl. Phys. Lett.* **83** 4005
[11] Wall J, Langmore J, Isaacson M and Crewe A V 1974 *Proc. Natl Acad. Sci. USA* **71** 105
[12] Sharma R 2005 *J. Mater. Res.* **20** 1695
[13] Hagen C W, Silvis-Cividjian N and Kruit P 2005 *Scanning* **27** 90
[14] Guise O, Marbach H, Levy J, Ahner J and Yates J T 2004 *Surf. Sci.* **571** 128
[15] Wang S, Sun Y M, Wang Q and White J M 2004 *J. Vac. Sci. Technol.* B **22** 1803
[16] Scheuer V, Koops H W P and Tschudi T 1986 *Microelectron. Eng.* **5** 423
[17] Hartel P, Rose H and Dinges C 1996 *Ultramicroscopy* **63** 93